Search for charged Higgs bosons in e^+e^- collisions at $\sqrt{s}$ = 172 GeV

P. Abreu, W. Adam, T. Adye, P. Adzic, G D. Alekseev, R. Alemany, P P. Allport, S. Almehed, U. Amaldi, S. Amato, et al.

EUROPEAN ORGANIZATION FOR NUCLEAR RESEARCH

CERN–PPE/97–145

20 November 1997

Search for charged Higgs bosons in e^+e^- collisions at $\sqrt{s} = 172$ GeV

DELPHI Collaboration

Abstract

This paper presents results on charged Higgs boson production, based on LEP data collected at $\sqrt{s} = 172$ GeV, that complement the previous DELPHI results obtained at centre of mass energies up to 161 GeV. The charged Higgs bosons are assumed to be pair produced and to decay either into a quark pair or into $\tau\nu_\tau$. The three different possible final states are included in the analysis. Data from ring imaging Cherenkov and microvertex detectors are used to identify the quarks as a cs pair. The number of candidates found is compatible with the background expected from standard processes. Combining the results of the present analysis with those of the previous analysis at lower energies, a new lower mass limit for the charged Higgs boson is set at 54.5 GeV/c^2.

(Submitted to Phys. Lett. B)

P.Abreu[21], W.Adam[49], T.Adye[36], P.Adzic[11], G.D.Alekseev[16], R.Alemany[48], P.P.Allport[22], S.Almehed[24], U.Amaldi[9], S.Amato[46], P.Andersson[43], A.Andreazza[9], P.Antilogus[25], W-D.Apel[17], Y.Arnoud[14], B.Åsman[43], J-E.Augustin[25], A.Augustinus[9], P.Baillon[9], P.Bambade[19], F.Barao[21], D.Y.Bardin[16], G.Barker[9], A.Baroncelli[39], O.Barring[24], M.J.Bates[36], M.Battaglia[15], M.Baubillier[23], J.Baudot[38], K-H.Becks[51], M.Begalli[6], P.Beilliere[8], Yu.Belokopytov[9,52], A.C.Benvenuti[5], C.Berat[14], M.Berggren[46], D.Bertini[25], D.Bertrand[2], M.Besancon[38], F.Bianchi[44], M.Bigi[44], M.S.Bilenky[16], P.Billoir[23], M-A.Bizouard[19], D.Bloch[10], M.Blume[51], M.Bonesini[27], W.Bonivento[27], M.Boonekamp[38], P.S.L.Booth[22], A.W.Borgland[4], G.Borisov[38], C.Bosio[39], O.Botner[47], E.Boudinov[30], B.Bouquet[19], C.Bourdarios[19], T.J.V.Bowcock[22], I.Bozovic[11], M.Bozzo[13], P.Branchini[39], K.D.Brand[35], T.Brenke[51], R.A.Brenner[47], R.Brown[9], P.Bruckman[35], J-M.Brunet[8], L.Bugge[32], T.Buran[32], T.Burgsmueller[51], P.Buschmann[51], S.Cabrera[48], M.Caccia[27], M.Calvi[27], A.J.Camacho Rozas[40], T.Camporesi[9], V.Canale[37], M.Canepa[13], F.Carena[9], L.Carroll[22], C.Caso[13], M.V.Castillo Gimenez[48], A.Cattai[9], F.R.Cavallo[5], Ch.Cerruti[10], V.Chabaud[9], N.Chalanda[41], Ph.Charpentier[9], L.Chaussard[25], P.Checchia[35], G.A.Chelkov[16], M.Chen[2], R.Chierici[44], P.Chochula[7], V.Chorowicz[25], J.Chudoba[29], V.Cindro[42], P.Collins[9], M.Colomer[48], R.Contri[13], E.Cortina[48], G.Cosme[19], F.Cossutti[45], J-H.Cowell[22], H.B.Crawley[1], D.Crennell[36], G.Crosetti[13], J.Cuevas Maestro[33], S.Czellar[15], B.Dalmagne[19], G.Damgaard[28], P.D.Dauncey[36], M.Davenport[9], W.Da Silva[23], A.Deghorain[2], G.Della Ricca[45], P.Delpierre[26], N.Demaria[34], A.De Angelis[9], W.De Boer[17], S.De Brabandere[2], C.De Clercq[2], C.De La Vaissiere[23], B.De Lotto[45], A.De Min[35], L.De Paula[46], H.Dijkstra[9], L.Di Ciaccio[37], A.Di Diodato[37], A.Djannati[8], J.Dolbeau[8], K.Doroba[50], M.Dracos[10], J.Drees[51], K.-A.Drees[51], M.Dris[31], J-D.Durand[25,9], D.Edsall[1], R.Ehret[17], G.Eigen[4], T.Ekelof[47], G.Ekspong[43], M.Ellert[47], M.Elsing[9], J-P.Engel[10], B.Erzen[42], M.Espirito Santo[21], E.Falk[24], G.Fanourakis[11], D.Fassouliotis[45], J.Fayot[23], M.Feindt[17], P.Ferrari[27], A.Ferrer[48], S.Fichet[23], A.Firestone[1], P.-A.Fischer[9], U.Flagmeyer[51], H.Foeth[9], E.Fokitis[31], F.Fontanelli[13], F.Formenti[9], B.Franek[36], A.G.Frodesen[4], R.Fruhwirth[49], F.Fulda-Quenzer[19], J.Fuster[48], A.Galloni[22], D.Gamba[44], M.Gandelman[46], C.Garcia[48], J.Garcia[40], C.Gaspar[9], M.Gaspar[46], U.Gasparini[35], Ph.Gavillet[9], E.N.Gazis[31], D.Gele[10], J-P.Gerber[10], L.Gerdyukov[41], F.Glege[51], R.Gokieli[50], B.Golob[42], P.Goncalves[21], G.Gopal[36], L.Gorn[1], M.Gorski[50], V.Gracco[13], E.Graziani[39], C.Green[22], A.Grefrath[51], P.Gris[38], G.Grosdidier[19], K.Grzelak[50], M.Gunther[47], J.Guy[36], Yu.Guz[41], F.Hahn[9], S.Hahn[51], S.Haider[9], Z.Hajduk[18], A.Hallgren[47], K.Hamacher[51], F.J.Harris[34], V.Hedberg[24], S.Heising[17], R.Henriques[21], J.J.Hernandez[48], P.Herquet[2], H.Herr[9], T.L.Hessing[34], J.-M.Heuser[51], E.Higon[48], S-O.Holmgren[43], P.J.Holt[34], D.Holthuizen[30], S.Hoorelbeke[2], M.Houlden[22], J.Hrubec[49], K.Huet[2], K.Hultqvist[43], J.N.Jackson[22], R.Jacobsson[43], P.Jalocha[9], R.Janik[7], Ch.Jarlskog[24], G.Jarlskog[24], P.Jarry[38], B.Jean-Marie[19], E.K.Johansson[43], L.Jonsson[24], P.Jonsson[24], C.Joram[9], P.Juillot[10], M.Kaiser[17], F.Kapusta[23], K.Karafasoulis[11], S.Katsanevas[25], E.C.Katsoufis[31], R.Keranen[4], B.A.Khomenko[16], N.N.Khovanski[16], B.King[22], N.J.Kjaer[30], O.Klapp[51], H.Klein[9], P.Kluit[30], D.Knoblauch[17], P.Kokkinias[11], M.Koratzinos[9], K.Korcyl[18], C.Kourkoumelis[3], O.Kouznetsov[16], M.Krammer[49], C.Kreuter[9], I.Kronkvist[24], J.Krstic[11], Z.Krumstein[16], P.Kubinec[7], W.Kucewicz[18], K.Kurvinen[15], C.Lacasta[9], I.Laktineh[25], J.W.Lamsa[1], L.Lanceri[45], D.W.Lane[1], P.Langefeld[51], J-P.Laugier[38], R.Lauhakangas[15], G.Leder[49], F.Ledroit[14], V.Lefebure[2], C.K.Legan[1], A.Leisos[11], R.Leitner[29], J.Lemonne[2], G.Lenzen[51], V.Lepeltier[19], T.Lesiak[18], M.Lethuillier[38], J.Libby[34], D.Liko[9], A.Lipniacka[43], I.Lippi[35], B.Loerstad[24], J.G.Loken[34], J.M.Lopez[40], D.Loukas[11], P.Lutz[38], L.Lyons[34], J.MacNaughton[49], J.R.Mahon[6], A.Maio[21], A.Malek[51], T.G.M.Malmgren[43], V.Malychev[16], F.Mandl[49], J.Marco[40], R.Marco[40], B.Marechal[46], M.Margoni[35], J-C.Marin[9], C.Mariotti[9], A.Markou[11], C.Martinez-Rivero[33], F.Martinez-Vidal[48], S.Marti i Garcia[22], F.Matorras[40], C.Matteuzzi[27], G.Matthiae[37], M.Mazzucato[35], M.Mc Cubbin[22], R.Mc Kay[1], R.Mc Nulty[9], G.Mc Pherson[22], J.Medbo[47], C.Meroni[27], W.T.Meyer[1], M.Michelotto[35], E.Migliore[44], L.Mirabito[25], W.A.Mitaroff[49], U.Mjoernmark[24], T.Moa[43], R.Moeller[28], K.Moenig[9], M.R.Monge[13], X.Moreau[23], P.Morettini[13], K.Muenich[51], M.Mulders[30], L.M.Mundim[6], W.J.Murray[36], B.Muryn[14,18], G.Myatt[34], T.Myklebust[32], F.Naraghi[14], F.L.Navarria[5], S.Navas[48], K.Nawrocki[50], P.Negri[27], S.Nemecek[12], N.Neufeld[9], W.Neumann[51], N.Neumeister[49], R.Nicolaidou[14], B.S.Nielsen[28], M.Nieuwenhuizen[30], V.Nikolaenko[10], M.Nikolenko[10,16], P.Niss[43], A.Nomerotski[35], A.Normand[22], A.Nygren[24], W.Oberschulte-Beckmann[17], A.G.Olshevski[16], A.Onofre[21], R.Orava[15], G.Orazi[10], S.Ortuno[48], K.Osterberg[15], A.Ouraou[38], P.Paganini[19], M.Paganoni[27], S.Paiano[5], R.Pain[23], R.Paiva[21], H.Palka[18], Th.D.Papadopoulou[31], K.Papageorgiou[11], L.Pape[9], C.Parkes[34], F.Parodi[13], U.Parzefall[22], A.Passeri[39], M.Pegoraro[35], L.Peralta[21], H.Pernegger[49], M.Pernicka[49], A.Perrotta[5], C.Petridou[45], A.Petrolini[13], H.T.Phillips[36], G.Piana[13], F.Pierre[38], M.Pimenta[21], E.Piotto[35], T.Podobnik[34], O.Podobrin[9], M.E.Pol[6], G.Polok[18], P.Poropat[45], V.Pozdniakov[16], P.Privitera[37], N.Pukhaeva[16], A.Pullia[27], D.Radojicic[34], S.Ragazzi[27], H.Rahmani[31], J.Rames[12], P.N.Ratoff[20], A.L.Read[32], P.Rebecchi[9], N.G.Redaelli[27], M.Regler[49], D.Reid[9], R.Reinhardt[51], P.B.Renton[34], L.K.Resvanis[3], F.Richard[19], J.Ridky[12], G.Rinaudo[44], O.Rohne[32], A.Romero[44], P.Ronchese[35], E.I.Rosenberg[1], P.Rosinsky[7], P.Roudeau[19], T.Rovelli[5], V.Ruhlmann-Kleider[38], A.Ruiz[40], H.Saarikko[15], Y.Sacquin[38], A.Sadovsky[16], G.Sajot[14], J.Salt[48], D.Sampsonidis[11], M.Sannino[13], H.Schneider[17], U.Schwickerath[17], M.A.E.Schyns[51], F.Scuri[45], P.Seager[20], Y.Sedykh[16], A.M.Segar[34], A.Seitz[17], R.Sekulin[36], V.Senko[41], R.C.Shellard[6], A.Sheridan[22], P.Siegrist[9,38], R.Silvestre[38], F.Simonetto[35], A.N.Sisakian[16], T.B.Skaali[32], G.Smadja[25], O.Smirnova[24], G.R.Smith[36], O.Solovianov[41], R.Sosnowski[50], D.Souza-Santos[6], T.Spassov[21], E.Spiriti[39], P.Sponholz[51], S.Squarcia[13], D.Stampfer[9], C.Stanescu[39], S.Stanic[42], S.Stapnes[32], I.Stavitski[35], K.Stevenson[34], A.Stocchi[19], J.Strauss[49], R.Strub[10], B.Stugu[4], M.Szczekowski[50], M.Szeptycka[50], T.Tabarelli[27], F.Tegenfeldt[47], F.Terranova[27], J.Thomas[34], A.Tilquin[26], J.Timmermans[30], L.G.Tkatchev[16], T.Todorov[10], S.Todorova[10], D.Z.Toet[30], A.Tomaradze[2], B.Tome[21], A.Tonazzo[27], L.Tortora[39], G.Transtromer[24],

D.Treille[9], G.Tristram[8], A.Trombini[19], C.Troncon[27], A.Tsirou[9], M-L.Turluer[38], I.A.Tyapkin[16], M.Tyndel[36], S.Tzamarias[11], B.Ueberschaer[51], O.Ullaland[9], G.Valenti[5], E.Vallazza[45], C.Vander Velde[2], G.W.Van Apeldoorn[30], P.Van Dam[30], W.K.Van Doninck[2], J.Van Eldik[30], A.Van Lysebetten[2], I.Van Vulpen[30], N.Vassilopoulos[34], G.Vegni[27], L.Ventura[35], W.Venus[36], F.Verbeure[2], M.Verlato[35], L.S.Vertogradov[16], V.Verzi[37], D.Vilanova[38], P.Vincent[23], N.Vishnevsky[41], L.Vitale[45], A.S.Vodopyanov[16], V.Vrba[12], H.Wahlen[51], C.Walck[43], F.Waldner[45], C.Weiser[17], A.M.Wetherell[9], D.Wicke[51], J.H.Wickens[2], G.R.Wilkinson[9], W.S.C.Williams[34], M.Winter[10], M.Witek[18], T.Wlodek[19], G.Wolf[9], J.Yi[1], F.Zach[25], A.Zalewska[18], P.Zalewski[50], D.Zavrtanik[42], E.Zevgolatakos[11], N.I.Zimin[16], G.C.Zucchelli[43], G.Zumerle[35]

[1] Department of Physics and Astronomy, Iowa State University, Ames IA 50011-3160, USA
[2] Physics Department, Univ. Instelling Antwerpen, Universiteitsplein 1, BE-2610 Wilrijk, Belgium
and IIHE, ULB-VUB, Pleinlaan 2, BE-1050 Brussels, Belgium
and Faculté des Sciences, Univ. de l'Etat Mons, Av. Maistriau 19, BE-7000 Mons, Belgium
[3] Physics Laboratory, University of Athens, Solonos Str. 104, GR-10680 Athens, Greece
[4] Department of Physics, University of Bergen, Allégaten 55, NO-5007 Bergen, Norway
[5] Dipartimento di Fisica, Università di Bologna and INFN, Via Irnerio 46, IT-40126 Bologna, Italy
[6] Centro Brasileiro de Pesquisas Físicas, rua Xavier Sigaud 150, BR-22290 Rio de Janeiro, Brazil
and Depto. de Física, Pont. Univ. Católica, C.P. 38071 BR-22453 Rio de Janeiro, Brazil
and Inst. de Física, Univ. Estadual do Rio de Janeiro, rua São Francisco Xavier 524, Rio de Janeiro, Brazil
[7] Comenius University, Faculty of Mathematics and Physics, Mlynska Dolina, SK-84215 Bratislava, Slovakia
[8] Collège de France, Lab. de Physique Corpusculaire, IN2P3-CNRS, FR-75231 Paris Cedex 05, France
[9] CERN, CH-1211 Geneva 23, Switzerland
[10] Institut de Recherches Subatomiques, IN2P3 - CNRS/ULP - BP20, FR-67037 Strasbourg Cedex, France
[11] Institute of Nuclear Physics, N.C.S.R. Demokritos, P.O. Box 60228, GR-15310 Athens, Greece
[12] FZU, Inst. of Phys. of the C.A.S. High Energy Physics Division, Na Slovance 2, CZ-180 40, Praha 8, Czech Republic
[13] Dipartimento di Fisica, Università di Genova and INFN, Via Dodecaneso 33, IT-16146 Genova, Italy
[14] Institut des Sciences Nucléaires, IN2P3-CNRS, Université de Grenoble 1, FR-38026 Grenoble Cedex, France
[15] Helsinki Institute of Physics, HIP, P.O. Box 9, FI-00014 Helsinki, Finland
[16] Joint Institute for Nuclear Research, Dubna, Head Post Office, P.O. Box 79, RU-101 000 Moscow, Russian Federation
[17] Institut für Experimentelle Kernphysik, Universität Karlsruhe, Postfach 6980, DE-76128 Karlsruhe, Germany
[18] Institute of Nuclear Physics and University of Mining and Metalurgy, Ul. Kawiory 26a, PL-30055 Krakow, Poland
[19] Université de Paris-Sud, Lab. de l'Accélérateur Linéaire, IN2P3-CNRS, Bât. 200, FR-91405 Orsay Cedex, France
[20] School of Physics and Chemistry, University of Lancaster, Lancaster LA1 4YB, UK
[21] LIP, IST, FCUL - Av. Elias Garcia, 14-1^{o}, PT-1000 Lisboa Codex, Portugal
[22] Department of Physics, University of Liverpool, P.O. Box 147, Liverpool L69 3BX, UK
[23] LPNHE, IN2P3-CNRS, Univ. Paris VI et VII, Tour 33 (RdC), 4 place Jussieu, FR-75252 Paris Cedex 05, France
[24] Department of Physics, University of Lund, Sölvegatan 14, SE-223 63 Lund, Sweden
[25] Université Claude Bernard de Lyon, IPNL, IN2P3-CNRS, FR-69622 Villeurbanne Cedex, France
[26] Univ. d'Aix - Marseille II - CPP, IN2P3-CNRS, FR-13288 Marseille Cedex 09, France
[27] Dipartimento di Fisica, Università di Milano and INFN, Via Celoria 16, IT-20133 Milan, Italy
[28] Niels Bohr Institute, Blegdamsvej 17, DK-2100 Copenhagen Ø, Denmark
[29] NC, Nuclear Centre of MFF, Charles University, Areal MFF, V Holesovickach 2, CZ-180 00, Praha 8, Czech Republic
[30] NIKHEF, Postbus 41882, NL-1009 DB Amsterdam, The Netherlands
[31] National Technical University, Physics Department, Zografou Campus, GR-15773 Athens, Greece
[32] Physics Department, University of Oslo, Blindern, NO-1000 Oslo 3, Norway
[33] Dpto. Fisica, Univ. Oviedo, Avda. Calvo Sotelo s/n, ES-33007 Oviedo, Spain, (CICYT-AEN96-1681)
[34] Department of Physics, University of Oxford, Keble Road, Oxford OX1 3RH, UK
[35] Dipartimento di Fisica, Università di Padova and INFN, Via Marzolo 8, IT-35131 Padua, Italy
[36] Rutherford Appleton Laboratory, Chilton, Didcot OX11 OQX, UK
[37] Dipartimento di Fisica, Università di Roma II and INFN, Tor Vergata, IT-00173 Rome, Italy
[38] DAPNIA/Service de Physique des Particules, CEA-Saclay, FR-91191 Gif-sur-Yvette Cedex, France
[39] Istituto Superiore di Sanità, Ist. Naz. di Fisica Nucl. (INFN), Viale Regina Elena 299, IT-00161 Rome, Italy
[40] Instituto de Fisica de Cantabria (CSIC-UC), Avda. los Castros s/n, ES-39006 Santander, Spain, (CICYT-AEN96-1681)
[41] Inst. for High Energy Physics, Serpukov P.O. Box 35, Protvino, (Moscow Region), Russian Federation
[42] J. Stefan Institute, Jamova 39, SI-1000 Ljubljana, Slovenia and Department of Astroparticle Physics, School of Environmental Sciences, Kostanjeviska 16a, Nova Gorica, SI-5000 Slovenia,
and Department of Physics, University of Ljubljana, SI-1000 Ljubljana, Slovenia
[43] Fysikum, Stockholm University, Box 6730, SE-113 85 Stockholm, Sweden
[44] Dipartimento di Fisica Sperimentale, Università di Torino and INFN, Via P. Giuria 1, IT-10125 Turin, Italy
[45] Dipartimento di Fisica, Università di Trieste and INFN, Via A. Valerio 2, IT-34127 Trieste, Italy
and Istituto di Fisica, Università di Udine, IT-33100 Udine, Italy
[46] Univ. Federal do Rio de Janeiro, C.P. 68528 Cidade Univ., Ilha do Fundão BR-21945-970 Rio de Janeiro, Brazil
[47] Department of Radiation Sciences, University of Uppsala, P.O. Box 535, SE-751 21 Uppsala, Sweden
[48] IFIC, Valencia-CSIC, and D.F.A.M.N., U. de Valencia, Avda. Dr. Moliner 50, ES-46100 Burjassot (Valencia), Spain
[49] Institut für Hochenergiephysik, Österr. Akad. d. Wissensch., Nikolsdorfergasse 18, AT-1050 Vienna, Austria
[50] Inst. Nuclear Studies and University of Warsaw, Ul. Hoza 69, PL-00681 Warsaw, Poland
[51] Fachbereich Physik, University of Wuppertal, Postfach 100 127, DE-42097 Wuppertal, Germany
[52] On leave of absence from IHEP Serpukhov

1 Introduction

In the simplest extension of the Standard Model (SM), with two Higgs field doublets, there are two charged and three neutral physical Higgs bosons. The Minimal Supersymmetric Standard Model (MSSM), which has the potential of solving the outstanding naturalness and hierarchy problems of the SM, is a particular case of such an extension. The discovery of charged Higgs bosons would provide evidence for the scheme of two Higgs field doublets.

A search has been performed for charged Higgs bosons based on the data collected with the DELPHI detector at LEP. The analysis described in this paper is based on 8.9 pb^{-1} of data collected at an e^+e^- centre of mass energy $\sqrt{s}$ = 172 GeV, and 1.1 pb^{-1} collected at $\sqrt{s}$ = 170 GeV. The results are combined with those from the data collected at $\sqrt{s}$ = 130–136 GeV and $\sqrt{s}$ = 161 GeV [1] to set new lower mass limits for the charged Higgs boson.

When searching for charged Higgs bosons, the rejection of the W^+W^- background becomes increasingly difficult as $\sqrt{s}$ grows above the W^+W^- production threshold at 161 GeV. In order to increase the rejection power in the analysis, an additional feature, namely the particle identification information from the ring imaging Cherenkov (RICH) and microvertex detectors in DELPHI, was therefore used to tag the s and c quarks in the hadronic decay of the charged Higgs boson.

The other features of the analysis are similar to those of the analysis described in detail in [1]. The DELPHI detector and its performance are described in detail in [2,3].

2 The Analysis

2.1 Particle Selection

Charged particles were selected if their momenta were greater than 100 MeV/c and their impact parameters were below 10 cm along the beam axis and 4 cm in the plane transverse to the beam. Charged particles were assigned the $\pi^{\pm}$ mass. Neutral particles with energy deposits in the hadronic calorimeter were selected if their total energy was greater than 400 MeV. Such particles were assigned the K^0 mass. Other neutral particles were selected if the energy deposited in the electromagnetic calorimeter was greater than 200 MeV. Such particles were assigned zero mass.

2.2 The Hadronic Channel

In the hadronic channel, each of the charged Higgs bosons decays into a cs pair. The topology of such an event is determined by the presence of four hadronic jets. After an initial four-jet selection, a Fisher discriminant analysis [4,5] was performed to accept 80% of the signal events while suppressing half of the background. The final selection used a kinematic fit imposing the two boson candidates in the event to be of equal mass.

2.2.1 Four Jet Selection

As in [1], an event was selected if its charged multiplicity was at least 12, its charged energy exceeded $0.30\sqrt{s}$, and its total energy exceeded $0.40\sqrt{s}$. These cuts were designed to eliminate almost all Bhabha and $\gamma\gamma$ events without affecting the signal. In order to reject initial state radiation, events with a detected or undetected photon with an energy

above 35 GeV were rejected. The energy of the undetected photon was reconstructed assuming energy and momentum conservation and that the photon direction was along the beam axis.

The sum of the 2nd and 4th Fox-Wolfram moments [6] of the event had to be below 1.1. The event was then clustered into 4 jets using the JADE algorithm [7], and the JADE parameter y_{43}, defined as the smallest value of $2E_iE_j(1-\cos\theta_{ij})/E^2_{\rm vis}$ for any two jets i and j in the four-jet event, was required to be larger than 0.004. Each jet also had to contain at least 2 charged particles.

The product of the smallest angle between two jets and the smallest jet energy was required to be greater than 6 GeV·rad, to suppress events with soft gluon radiation. A four constraint fit requiring energy and momentum conservation was then applied and the χ^2 of the fit had to be lower than 14 (3.5 per degree of freedom). After this four-jet selection, only $\mathrm{q\bar{q}}(\gamma)$, $\mathrm{W^+W^-}$ and $\mathrm{ZZ^*}$ background remained in the simulation (see the first row in Table 1).

2.2.2 Fisher Analysis

The input to the Fisher discriminant analysis was a signal sample of 1200 simulated events that had been obtained by applying the four-jet selection criteria to six signal samples of equal statistics, each with a different charged-Higgs mass in the range 44–60 GeV/c^2, and a background sample of 1200 simulated events with the relative composition of $\mathrm{q\bar{q}}(\gamma)$, $\mathrm{W^+W^-}$ and $\mathrm{ZZ^*}$ events that is expected after the four-jet selection. The variables $\lg(y_{43})$, $\theta_{\rm thrust}$, $P(\mathrm{c})$ and $f_{\rm K}$ used in the Fisher analysis are described below.

Since jets from radiated gluons tend to have small energies and small angles with respect to the jet of the radiating quark, true four-quark events tend to have a larger value of the JADE parameter y_{43} than two-quark events with two radiated gluons.

The angle $\theta_{\rm thrust}$ is the event thrust polar angle measured in radians and defined to be between 0 and $\frac{\pi}{2}$. This is an estimator of the production angle of the produced particle pair. Since the charged Higgs boson has spin 0, its differential production cross-section is proportional to $\sin^2\theta$, while $\mathrm{q\bar{q}}(\gamma)$ and $\mathrm{W^+W^-}$ events have angular distributions that are not peaked around 90°.

The event c quark probability, $P(\mathrm{c})$, is the normalised product of the probabilities for all tracks in the event to result from a charm decay, based on measurements of their impact parameters, momenta, and angles with respect to the jet axis (using the DELPHI `AABTAG` analysis package [8]). Since there are two c quarks in each signal event, this probability is expected to be higher for the signal than for the average background.

The variable $f_{\rm K}$ is derived from the particle identification information of the RICH detectors in DELPHI. For each jet, the fastest identified charged kaon was tagged using the "loose kaon tag" criteria of the DELPHI `NEWTAG` routine [9,10], which requires the measured value of the Cherenkov angle $\theta_{\rm c}$ of the particle to be compatible with that of a kaon of the measured momentum and separated by at least one standard deviation from the $\theta_{\rm c}$ values to be expected for a pion or proton of the same momentum. The momenta of these kaons are then summed provided the kaon is among the three fastest charged particles in its jet. $f_{\rm K}$ is this sum divided by $\sqrt{s}$. Since there are two s quarks and two c quarks in a signal event, their jets are more likely to contain fast kaons than are jets in average background events, implying a higher value for $f_{\rm K}$.

From a first trial, in which many more variables were studied in a Fisher analysis of simulated events, these four variables were selected in the above order as being the most effective variables in an $\mathrm{H^+H^-}$ search at $\sqrt{s}$ = 172 GeV, above the $\mathrm{W^+W^-}$ threshold. As a first step in the variable selection process, variables which were highly correlated

were grouped together. The variable with the highest separation power in each group was then selected for further use. It is notable that the particle identification variables, $P(\mathrm{c})$ and f_{K}, added in the present analysis, have been selected by this procedure. Running the Fisher analysis with these four variables only, yielded the following discriminating function:

$$F = 1.4112\ \lg(y_{43}) + 1.0923\ \theta_{\mathrm{thrust}} + 1.0739\ P(\mathrm{c}) + 3.9545\ \mathrm{f_K}\ . \qquad (1)$$

The distributions of the four individual Fisher variables for the simulated background and signal as well as for the data are shown in Figs. 1 and 2. The distributions for the combined Fisher discriminant are shown in Fig. 3. The agreement between total simulated background and data, for the Fisher discriminant as well as for each of the four variables, is satisfactory. The selectivity of the four individual variables and F is apparent from these figures: significant differences between signal and background are observed in each case.

By requiring $F > -0.65$ (optimised using the simulation to give the best expected mass limit), 80% of the signal events passing the four-jet selection in the simulated sample were kept whereas about 50% of the background events were suppressed. The signal purity obtained for a charged Higgs boson with a mass of 50 GeV/c^2 in a mass window of ± 2.64 GeV/c^2 ($\pm 2\sigma_m$ as discussed below) was 47.4% for a signal efficiency of 34.8%.

2.2.3 Kinematic Fit

A five constraint kinematic fit was then performed requiring energy and momentum conservation and the pair production of two objects of equal mass (i.e. the two charged Higgs boson candidates). Of the three possible jet pairings the one resulting in the smallest χ^2 was chosen. This χ^2 had to be smaller than 12.5 (2.5 per degree of freedom) for the event to be accepted.

The mass resolution of the fit was obtained by plotting the difference between the generated and reconstructed masses for all simulated events passing all the cuts. The peak of this histogram was then fitted to a zero-centred Gaussian over the range ± 3 GeV/c^2. This gave a standard error in mass of $\sigma_m = 1.32$ GeV/c^2. A mass window spanning $\pm 2\sigma_m$ around the generated mass was used to calculate the signal efficiencies and expected backgrounds.

The results of the analysis of the hadronic channel are shown in Fig. 4 and Tables 1 and 2. The agreement between simulated and real data is satisfactory. From Table 1 it is seen that, after the last step in background rejection, $\mathrm{W^+W^-}$ represents 74% of the remaining background and the signal efficiency is 51.8%. The $\mathrm{W^+W^-}$ mass peak is clearly visible in the top plot of Fig. 4. The tail extending down to approximately 30 GeV/c^2 in the top plot is due to $\mathrm{W^+W^-}$ background events for which the jet pairing has been done incorrectly. Likewise, the tail extending up to approximately 40 GeV/c^2 in the bottom plot is due to $\mathrm{H^+H^-}$ events with the wrong jet pairing.

Table 2 shows the mass window used for each generated $\mathrm{H^\pm}$ mass, the estimated background and the signal efficiencies with errors. It also shows the expected number of signal events for a branching ratio of charged Higgs bosons into hadrons of 1.0.

2.3 The Semi-Leptonic Channel

In the semi-leptonic channel one of the charged Higgs bosons decays into a cs pair and the other into a $\tau\nu_\tau$ pair. The topology of such an event is determined by the presence

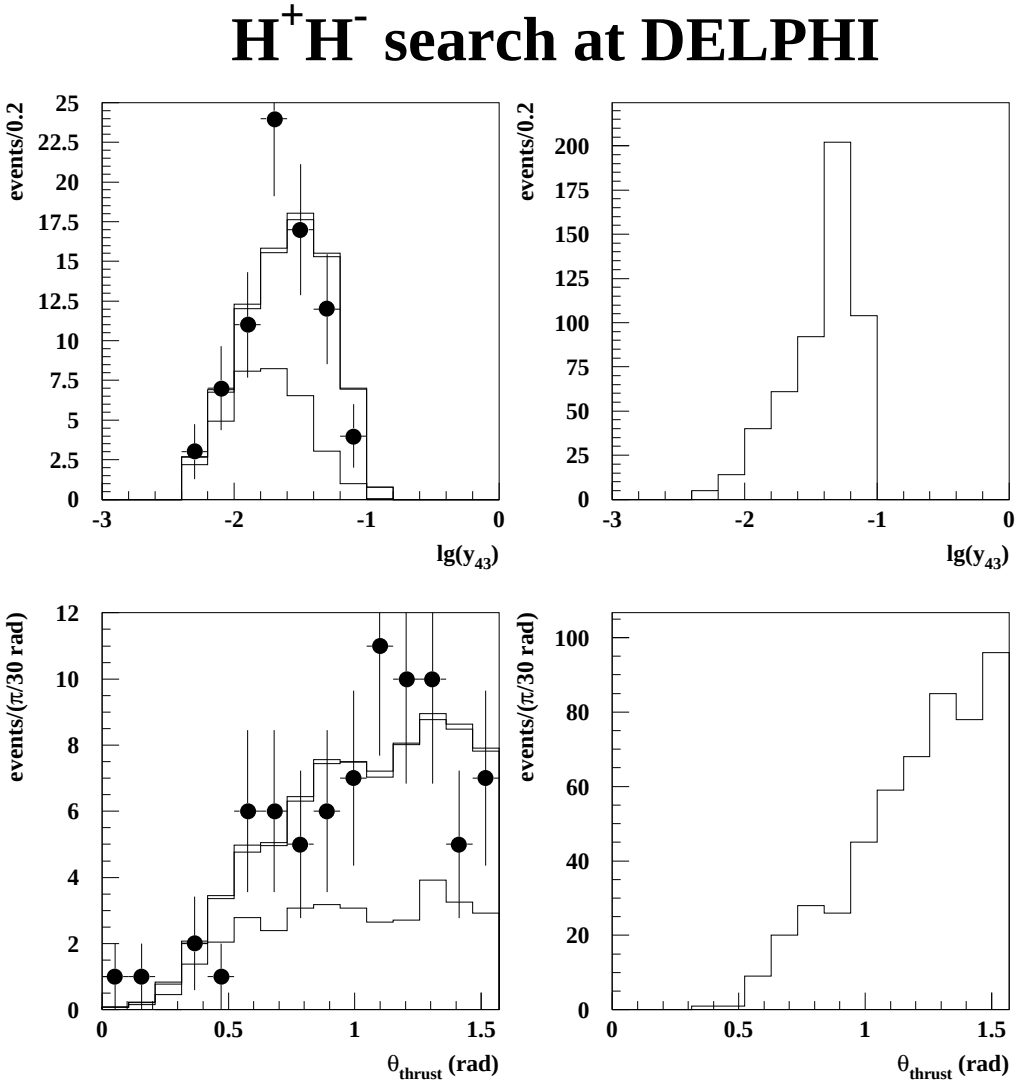

Figure 1: The histograms show the distributions of $\lg(y_{43})$ and $\theta_{\rm thrust}$ for the background (left) and the signal (right) in the hadronic channel. The background contributions from $q\bar{q}(\gamma)$ (bottom part of histogram), W^+W^- (middle part) and ZZ^* (top part) are shown separately. The dots with error bars show the distribution of the data.

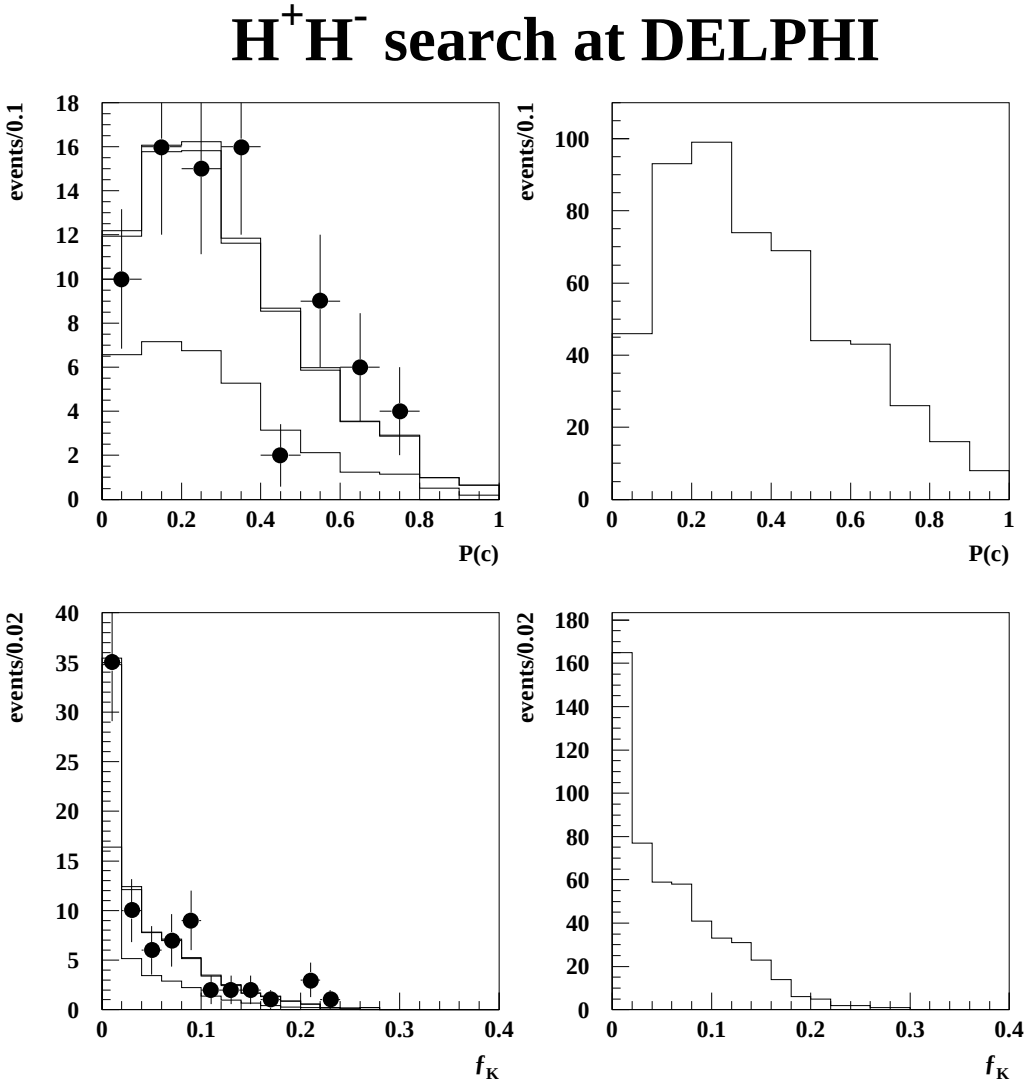

Figure 2: The histograms show the distributions of $P(\mathrm{c})$ and f_K for the background (left) and the signal (right) in the hadronic channel. The background contributions from $\mathrm{q\bar{q}}(\gamma)$ (bottom part of histogram), $\mathrm{W^+W^-}$ (middle part) and $\mathrm{ZZ^*}$ (top part) are shown separately. The dots with error bars show the distribution of the data.

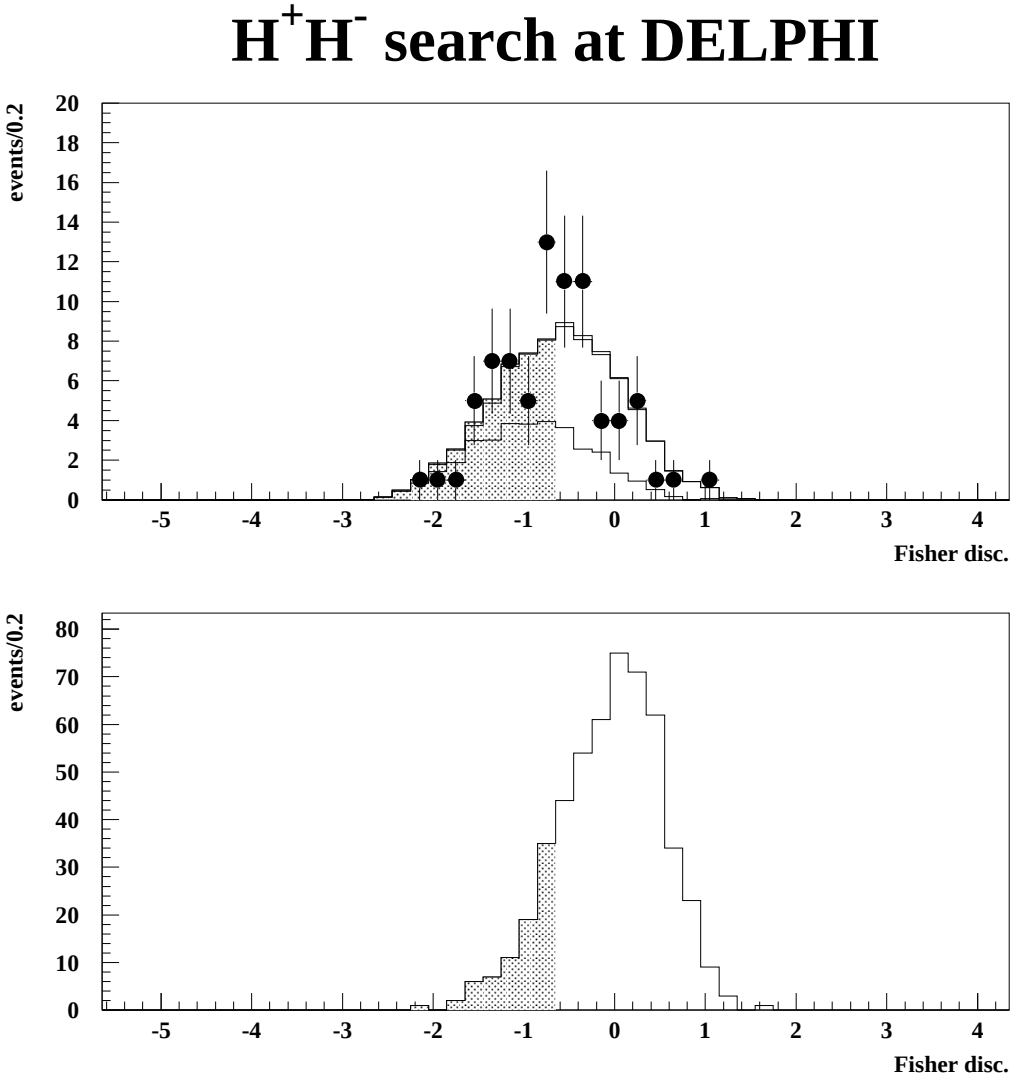

Figure 3: Top: the value of the Fisher discriminant in the hadronic channel for the simulated background and the data. The background contributions from $q\bar{q}(\gamma)$ (bottom part of histogram), W^+W^- (middle part) and ZZ^* (top part) are shown separately. The dots with error bars represent the data. Bottom: the same for a signal of a 50 GeV/c^2 charged Higgs. The shaded areas in the histograms are rejected by the cut at -0.65.

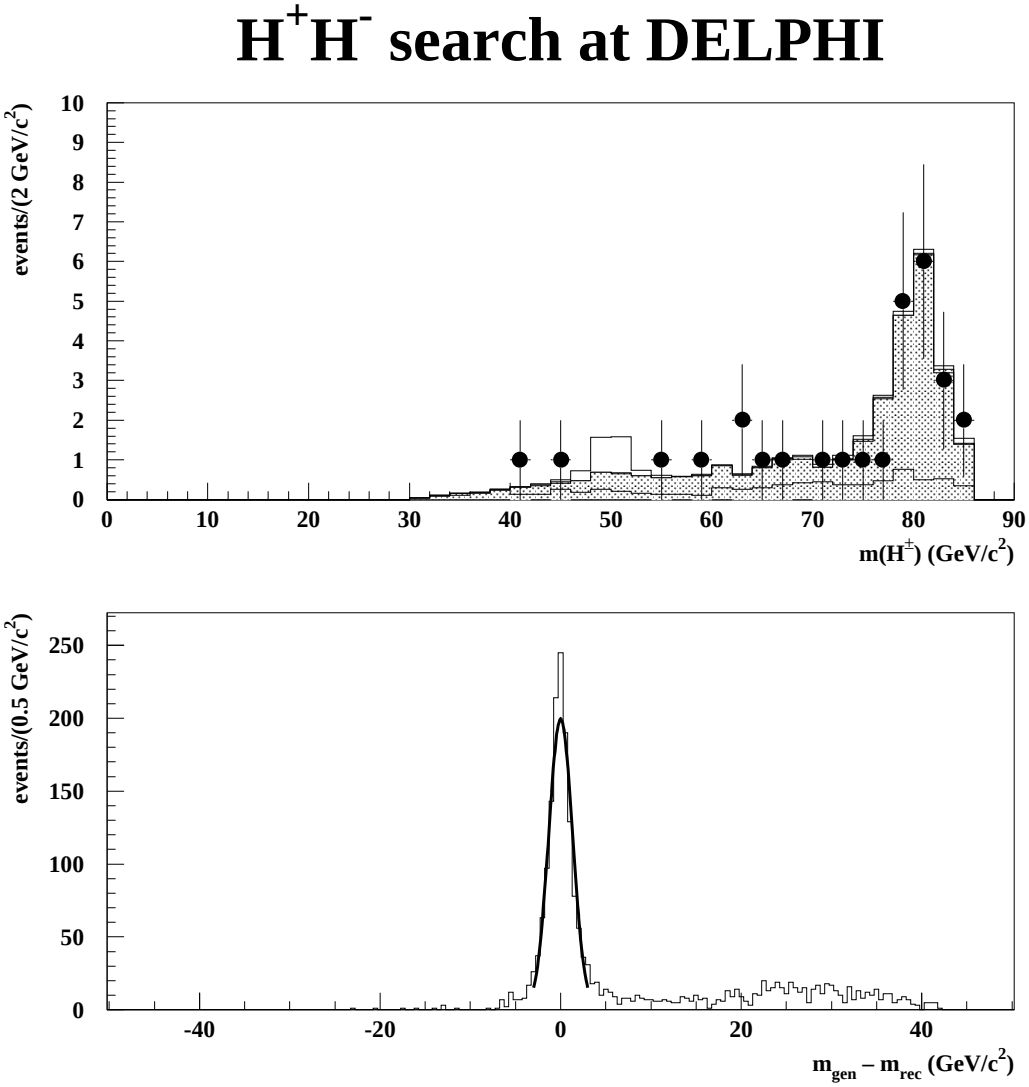

Figure 4: Top: The simulated background mass spectrum in the hadronic channel (grey histogram) and the real data (dots). The background contributions from $q\bar{q}(\gamma)$ (bottom part of histogram), W^+W^- (middle part) and ZZ^* (top part) are shown separately. The clear histogram on top of the background prediction shows the expected signal from charged Higgs bosons with a mass of 50 GeV/c^2 for a branching ratio of charged Higgs bosons into hadrons of 1. Bottom: the difference between the generated and reconstructed masses of simulated charged Higgs bosons passing all the cuts, and the Gaussian fit, which has a standard deviation of $\sigma_m = 1.32$ GeV/c^2.

Cut	Data	MC	$q\bar{q}(\gamma)$	W^+W^-	ZZ^*	Eff. (%)
4 jet sel.	78	79.1±1.5	34.1	43.5	1.47	69.2
Fisher	38	41.7±1.0	11.7	29.3	0.72	58.3
χ^2	28	$31.9\pm0.9^{+2.0}_{-2.0}$	7.8	23.7	0.46	51.8

Table 1: Total numbers of data and expected background events after the different cuts in the hadronic channel. The efficiencies given in the last column are for a charged Higgs boson with a mass of 50 GeV/c^2. Where present, the first error is statistical and the second systematic (see section 3).

$m_{H^\pm}$	Mass window	Data	Background	Eff. (%)	Signal
44	41.36–46.64	1	$1.05 \pm 0.16^{+0.07}_{-0.06}$	$28.6 \pm 2.0^{+1.0}_{-1.1}$	2.25
47	44.36–49.64	1	$1.40 \pm 0.19^{+0.09}_{-0.13}$	$23.7 \pm 1.8^{+1.0}_{-0.7}$	1.64
50	47.36–52.64	0	$1.65 \pm 0.20^{+0.10}_{-0.15}$	$32.7 \pm 2.1^{+0.9}_{-0.9}$	2.03
53	50.36–55.64	0	$1.67 \pm 0.20^{+0.10}_{-0.15}$	$27.1 \pm 1.9^{+1.4}_{-0.8}$	1.49
56	53.36–58.64	1	$1.52 \pm 0.20^{+0.11}_{-0.09}$	$28.4 \pm 1.9^{+0.8}_{-0.9}$	1.37
60	57.36–62.64	1	$1.80 \pm 0.25^{+0.12}_{-0.14}$	$30.1 \pm 2.0^{+0.8}_{-1.1}$	1.19

Table 2: The mass windows used for the different $H^\pm$ masses in the hadronic channel, the number of data events, the expected number of background events within these mass windows and the efficiency for the H^+H^- signal according to the simulation. The first error is statistical, the second systematic. The last column shows the number of expected signal events for a branching ratio of charged Higgs bosons into hadrons of 1.0. The three candidates entering this table have reconstructed masses of 45.8, 55.8 and 59.1 GeV/c^2. The first of these three candidates enters in each of the two first mass windows.

of two hadronic jets, one τ jet and missing energy and momentum carried by neutrinos. After a preselection, which includes several criteria on the τ jet, a Fisher discriminant analysis was used to accept 80% of the signal while rejecting 90% of the background. As a last step a kinematic fit was used to reconstruct the mass of the produced bosons.

2.3.1 Preselection and Tagging of the τ

An event was selected if its charged multiplicity was at least 7, its charged energy higher than $0.15\sqrt{s}$ and its total energy higher than $0.25\sqrt{s}$. In order to reject two-jet events, the event was divided into two hemispheres by a plane perpendicular to the sphericity axis and the acollinearity of the two hemispheric jets was required to be larger than 9°. In order to reject initial state radiation, events with a detected photon with an energy above 35 GeV were rejected. The energy deposited in cones spanning 20° (30°) around the beam was required to be lower than $0.30\sqrt{s}$ ($0.50\sqrt{s}$).

Due to the lower multiplicity in this channel (with respect to the hadronic channel), events caused by cosmic particles constitute a background. In order to reject these events, at least one charged particle in the event had to have been detected by at least two layers of the vertex detector and to have impact parameters smaller than 0.25 cm along the beam axis and 0.2 cm in the plane transverse to the beam.

The event was then clustered into 3 jets using the JADE algorithm. The jet with the lowest charged multiplicity was taken as the τ jet. If two jets had the same charged

multiplicity the less energetic one was chosen. For the event to be accepted, the τ jet had to have a charged multiplicity between 1 and 3, a total multiplicity not exceeding 7, a total energy between $0.02\sqrt{s}$ and $0.35\sqrt{s}$, and the largest angle between two particles within the τ jet had to be lower than 30°.

2.3.2 Fisher Analysis

At this stage a Fisher discriminant analysis was performed. The input to the algorithm was a signal sample of 1200 simulated events that had been obtained by applying the previous selection criteria to six signal samples of equal statistics, each with a different charged-Higgs mass in the range 44–60 GeV/^{2}, and a background sample of 1200 simulated events with the relative composition of $q\bar{q}(\gamma)$, W^+W^- and ZZ^* events expected after the previous selection. The variables used in the Fisher analysis were:

- $\theta_{p_{\rm miss}}$, the polar angle of the missing momentum measured in radians and defined to be between 0 and $\frac{\pi}{2}$; it discriminates against radiative return $q\bar{q}(\gamma)$ events and is also sensitive to the differences in the production angular distributions of H^+H^- and W^+W^-,
- $\theta_{\rm jj}$, the angle between the two hadronic jets measured in radians; it discriminates against $q\bar{q}$ events with a soft gluon that have been wrongly tagged as a τ,
- y_{32}, the JADE cut value and
- $P(\rm c)$, the event c quark probability.

These four variables had been selected from a larger sample of variables as in the case of the hadronic channel. Running the Fisher analysis with these four variables only yielded the following discriminant function:

$$F = 1.8510\ \theta_{p_{\rm miss}} - 1.4708\ \theta_{\rm jj} + 0.3483\ \lg(y_{32}) + 0.7440\ P(\rm c)\ . \qquad (2)$$

By requiring $F > -1.00$ (optimised to give the best expected mass limit), 80% of the signal events passing the preselection were kept and about 90% of the background events were suppressed. The distributions of the Fisher discriminant for the simulated background and signal as well as for the data are shown in Fig. 5. The agreement between total simulated background and data is satisfactory.

2.3.3 Kinematic Fit

A five constraint kinematic fit was then performed requiring energy and momentum conservation and the pair production of two objects of equal mass. The three components of the ν_τ momentum and the magnitude of the τ momentum were treated as unmeasured variables, reducing the number of degrees of freedom of the fit to one. The χ^2 of the fit had to be smaller than 2.5 for an event to be accepted.

The mass resolution of the fit was obtained by plotting the difference between the generated and reconstructed masses for all simulated events passing all the cuts. The peak of this histogram was then fitted to a zero-centred Gaussian over the range ± 5 GeV/c^2. This gives a standard error in mass of $\sigma_m = 2.44$ GeV/c^2. A mass window spanning $\pm 2\sigma_m$ around the generated mass was used to calculate the signal efficiencies and expected backgrounds.

The results of the analysis of the semi-leptonic channel are shown in Fig. 6 and Tables 3 and 4. The agreement between simulated and real data is satisfactory. From Table 3 it is seen that, after the last step in background rejection, W^+W^- represents 48% of the remaining background and the signal efficiency is 41.1%.

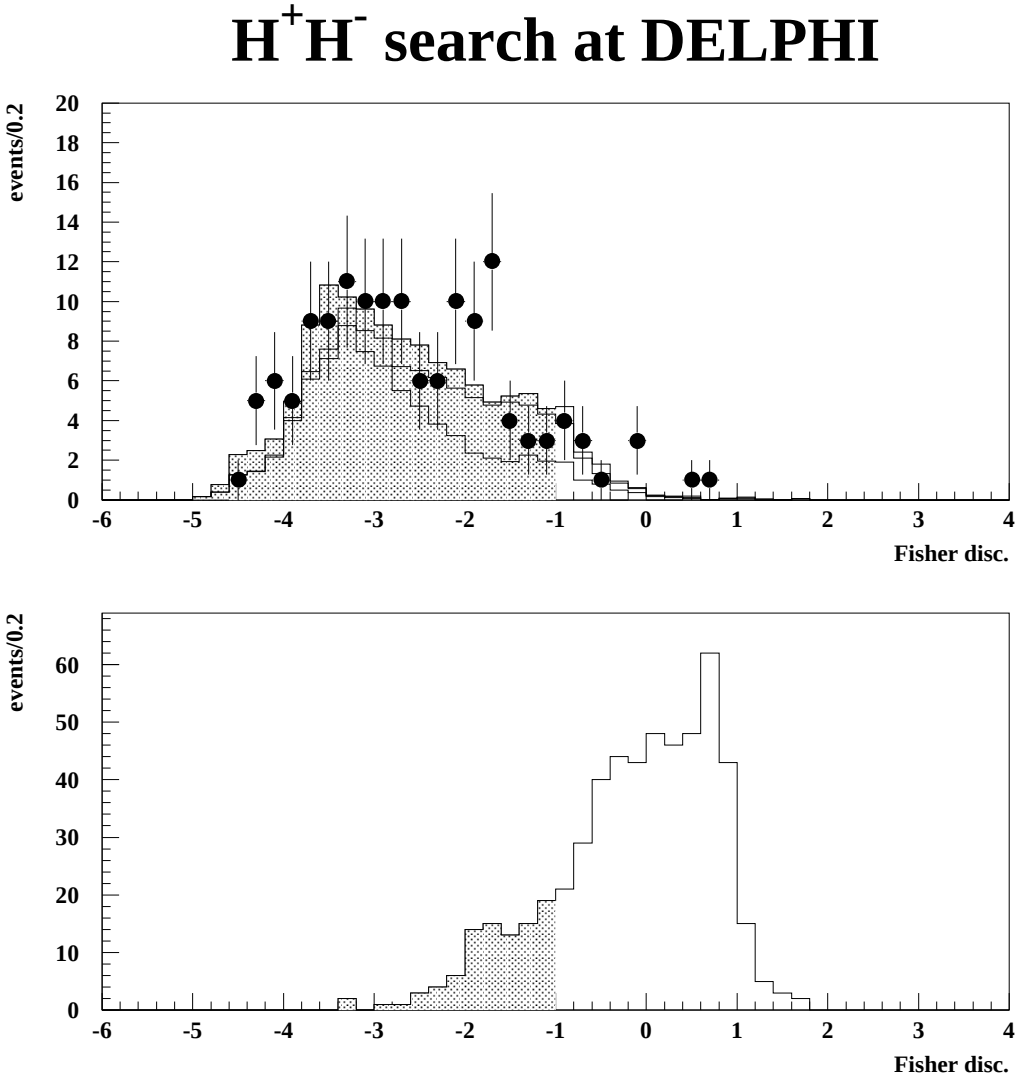

Figure 5: Top: the value of the Fisher discriminant in the semi-leptonic channel for the background and the data. The background contributions from $q\bar{q}(\gamma)$ (bottom part of histogram), W^+W^- (middle part) and other backgrounds (top part) are shown separately. The dots with error bars represent the data. Bottom: the same for a signal of a 50 GeV/c^2 charged Higgs. The shaded areas in the histograms are rejected by the cut at -1.00.

Table 4 shows the mass window used for each generated $H^{\pm}$ mass, the estimated background and the signal efficiencies with errors. It also shows the expected number of signal events for a branching ratio of charged Higgs bosons into hadrons of 0.5.

Cut	Data	MC	$q\bar{q}(\gamma)$	W^+W^-	$\gamma\gamma$	other	Eff. (%)
Presel.	142	128.8±2.8	78.6	30.0	15.0	5.14	55.5
Fisher	13	11.5±0.8	5.1	4.4	1.0	1.00	46.0
χ^2	8	$8.8\pm0.7^{+0.8}_{-0.6}$	3.4	4.2	0.7	0.52	41.1

Table 3: Data and expected background in total number of events after the different cuts in the semi-leptonic channel. The efficiencies stated in the last column are for a charged Higgs boson of mass 50 GeV/c^2. Where present, the first error is statistical and the second systematic.

$m_{H^{\pm}}$	Mass window	Data	Background	Eff. (%)	Signal
44	39.12–48.88	1	$0.52 \pm 0.12^{+0.08}_{-0.04}$	$33.9 \pm 1.8^{+0.5}_{-0.5}$	1.33
47	42.12–51.88	1	$0.47 \pm 0.11^{+0.06}_{-0.04}$	$32.8 \pm 1.8^{+0.7}_{-0.7}$	1.13
50	45.12–54.88	1	$0.35 \pm 0.09^{+0.05}_{-0.00}$	$31.2 \pm 1.8^{+0.4}_{-0.5}$	0.97
53	48.12–57.88	0	$0.33 \pm 0.09^{+0.03}_{-0.01}$	$32.7 \pm 1.8^{+1.1}_{-1.1}$	0.90
56	51.12–60.88	0	$0.27 \pm 0.08^{+0.03}_{-0.01}$	$29.3 \pm 1.7^{+0.6}_{-0.4}$	0.71
60	55.12–64.88	1	$0.46 \pm 0.11^{+0.03}_{-0.01}$	$27.4 \pm 1.7^{+0.5}_{-0.4}$	0.54

Table 4: The mass windows used for the different $H^{\pm}$ masses in the semi-leptonic channel. The number of data events and the expected number of background events within these mass windows and the efficiency for the H^+H^- signal. The first error is statistical, the second systematic. The last column shows the number of expected signal events for a branching ratio of charged Higgs bosons into hadrons of 0.5. The two candidates entering this table have reconstructed masses of 47.6 and 63.7 GeV/c^2. The first of these two candidates enters in each of the three first mass windows.

2.4 The Leptonic Channel

In the leptonic channel both charged Higgs bosons decay into a $\tau\nu_\tau$ pair. The topology of such an event is determined by the presence of two τ jets, most likely acollinear, and missing energy and momentum carried by neutrinos. After a preselection, several criteria were imposed on the τ jets and on the angle between these jets. No mass reconstruction is possible in this channel since four neutrinos are produced.

2.4.1 Preselection

In this channel, where the multiplicity of the events is low, a tighter selection was applied on the charged particles in order to avoid events with false tracks and events caused by cosmic particles. In this case the impact parameters had to be smaller than 2.5 cm along the beam axis and 1 cm in the plane transverse to the beam. In addition the length of the track had to be above 60 cm and the relative error of the momentum measurement below 100%.

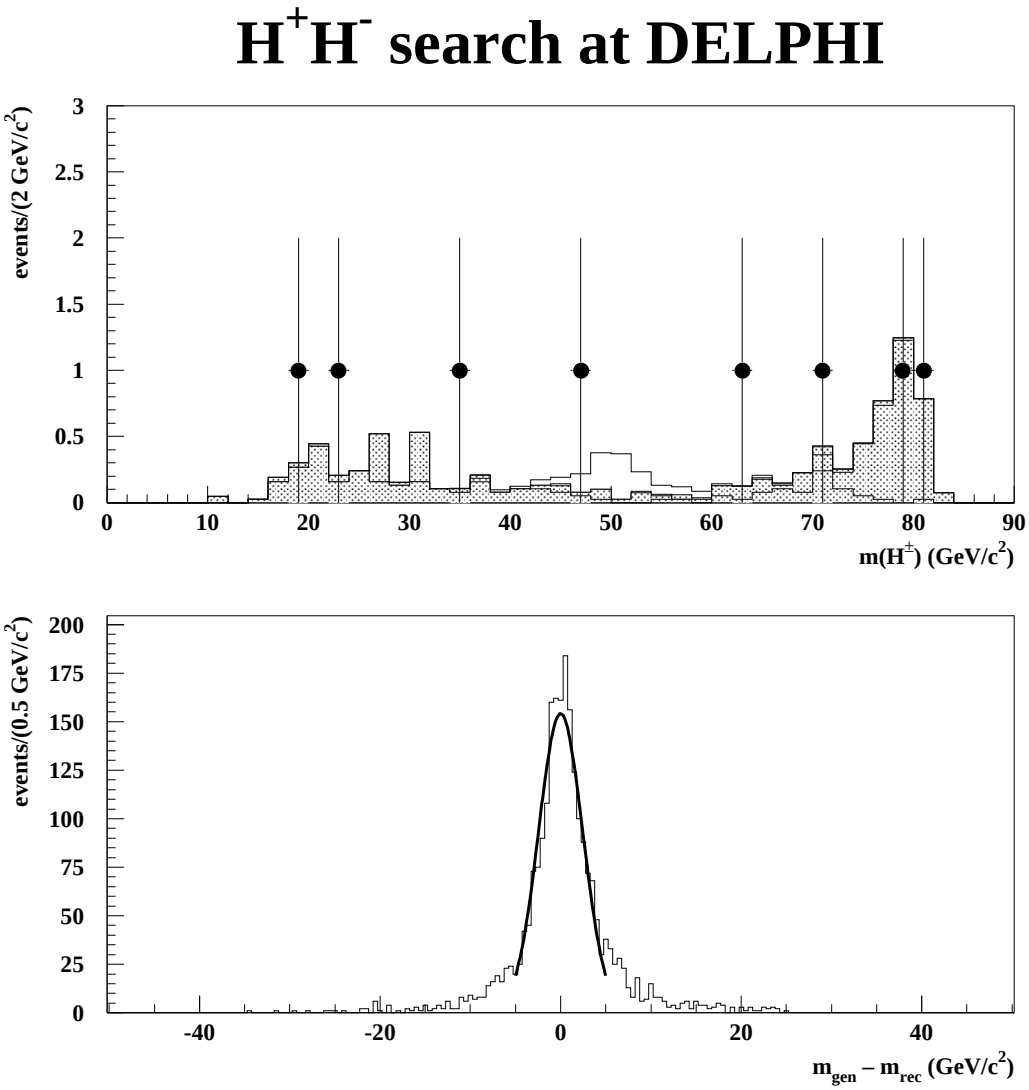

Figure 6: Top: The simulated background mass spectrum in the semi-leptonic channel (grey histogram) and the real data (dots). The background contributions from $q\bar{q}(\gamma)$ (bottom part of histogram), W^+W^- (middle part) and other backgrounds (top part) are shown separately. The clear histogram on top of the background prediction shows the expected signal from charged Higgs bosons with a mass of 50 GeV/c^2 for a branching ratio of charged Higgs bosons into hadrons of 0.5. Bottom: the difference between the generated and reconstructed masses of simulated charged Higgs bosons passing all the cuts, and the Gaussian fit, which has a standard deviation of $\sigma_m = 2.44$ GeV/c^2.

An event was selected if its charged multiplicity was between 2 and 6, its charged energy higher than $0.04\sqrt{s}$ and its total energy lower than $0.55\sqrt{s}$. In order to reject $\gamma\gamma$ background, the transverse momentum of the event had to be greater than $0.05\sqrt{s}/c$. The deposited energy in cones spanning 30° around the beam had to be lower than $0.10\sqrt{s}$, in order to reject Bhabha scattering events.

2.4.2 τ Jet Angles and Energies

The event was then clustered into two jets using the JADE algorithm. In order to reject $\gamma\gamma \longrightarrow \tau^+\tau^-$ events, the angle between the two jets to be greater than 20°. Events where the two jets are back to back were rejected by requiring this angle, and its projection on a plane perpendicular to the beam axis, to be below 167°.

Each jet had to contain at least one charged particle, and have a total energy above $0.02\sqrt{s}$, and the largest angle between two particles within a jet had to be smaller than 30° in order to enhance the selection of τ jets. To reduce the $\ell^+\ell^-(\gamma)$ and W^+W^- backgrounds containing prompt electrons and muons, the most (least) energetic jet had to have a total energy below $0.35\sqrt{s}$ ($0.18\sqrt{s}$).

The distributions, at preselection level, of the energy of the least energetic jet and of the angle between the two jets for the simulated background and signal as well as for the data are shown in Fig. 7. The agreement between the simulated background and the data is satisfactory.

The results of the analysis of the leptonic channel are shown in Tables 5 and 6. The agreement between simulated and real data is satisfactory. (The probability of finding one event or less when 4.23 events are expected, as obtained after the last step in background rejection, is 7.6%). After the last step in background rejection, W^+W^- represents 81% of the remaining background and the signal efficiency is 35%.

Cut	Data	MC	$f\bar{f}(\gamma)$	W^+W^-	$\gamma\gamma$	other	Eff. (%)
preselection	124	95.0±3.0	77.6	7.45	8.3	1.70	63.9
jet angles	9	12.2±0.7	2.9	6.66	1.8	0.81	56.0
jet energies	1	$4.23\pm0.36^{+0.23}_{-0.23}$	0.31	3.43	0.16	0.34	35.0

Table 5: Total number of data and expected background events after the different cuts in the leptonic channel. The efficiencies stated in the last column are for a charged Higgs boson of mass 50 GeV/c^2. Where present, the first error is statistical and the second systematic.

3 Systematic Errors

The systematic errors stated in Tables 1–6 were estimated by comparing the distributions of real and simulated data for each of the variables on which cuts were imposed to suppress the background. This study was done after the event preselection and also after the four-jet selection in the hadronic channel. For each variable, the effect of moving the cut on the variable by the difference between the average values of the real and simulated distributions was evaluated. The changes in efficiencies and background estimation thus obtained for each variable were added quadratically, and the results were taken as estimates of the corresponding systematic errors. The variables used for the study were:

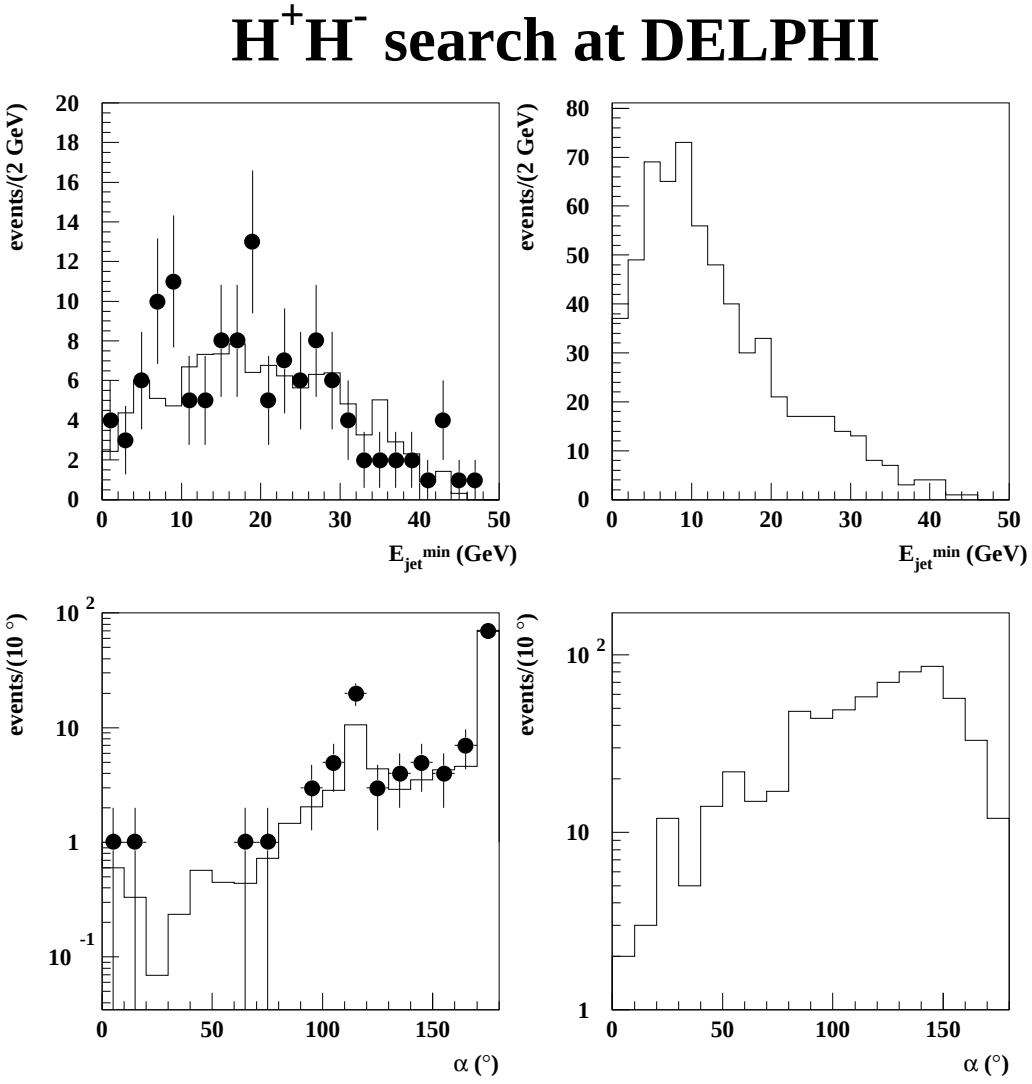

Figure 7: The histograms show the distributions of the energy of the least energetic jet (top) and the angle α between the two jets (bottom) for the background (left) and the signal (right) in the leptonic channel. The dots with error bars show the distribution of the data.

$m_{\mathrm{H}^{\pm}}$	Eff. (%)	Signal
44	$31.5 \pm 1.8^{+1.9}_{-2.1}$	2.48
47	$31.8 \pm 1.8^{+2.0}_{-2.2}$	2.20
50	$35.0 \pm 1.9^{+2.0}_{-2.0}$	2.17
53	$35.3 \pm 1.9^{+1.3}_{-1.5}$	1.94
56	$36.1 \pm 1.9^{+1.6}_{-1.6}$	1.74
60	$40.0 \pm 2.0^{+2.4}_{-2.5}$	1.58

Table 6: $\mathrm{H}^{+}\mathrm{H}^{-}$ efficiencies for charged Higgs bosons of different masses in the leptonic channel. The first error is statistical, the second systematic. The last column shows the number of expected signal events for a branching ratio of charged Higgs bosons into hadrons of 0.

a) in the hadronic channel the value of the Fisher discriminant, and the χ^2 of the five-constraint fit, b) in the semi-leptonic channel the acollinearity, the τ jet energy, the value of the Fisher discriminant and the χ^2 of the five constraint fit, and c) in the leptonic channel the transverse momentum and the τ jet energies and angles.

The systematic error of the four-jet selection used in the hadronic channel was studied previously [1] and amounts to $\pm 5.1\%$ of the background and $\pm 2.6\%$ of the efficiencies. These errors were added quadratically to the ones obtained as described above.

4 Exclusion Limits

The analysis described in this paper was combined with the analysis performed on the data collected at $\sqrt{s}$ = 130–136 GeV and $\sqrt{s}$ = 161 GeV described in [1]. The method used for combining the results from the different analyses is described in [11]. Each channel at each centre of mass energy is treated separately, giving in total 9 channels. For each channel the information about efficiency, expected background and number of candidates is used to derive a limit by using Bayesian statistics.

Exclusion mass limits for the charged Higgs boson were derived in the general scheme of two Higgs field doublets. In this scheme the production cross-section depends only on the mass of the charged Higgs boson. The result is shown in Fig. 8.

The influence of the downward fluctuation in the number of data events in the leptonic channel was evaluated by calculating what the limit would have been if the 4 candidates expected in this channel had been seen. The result is shown by the dashed line in Fig. 8.

5 Conclusions

A search for charged Higgs bosons was performed in the data collected by DELPHI at $\sqrt{s}$ = 172 GeV. The number of candidates found is compatible with the background expected from standard processes. The result of the analysis was combined with the results obtained at $\sqrt{s}$ = 130–136 GeV and $\sqrt{s}$ = 161 GeV [1]. From the analysis of the combined results, the existence of charged Higgs bosons is excluded at a confidence level of 95% for masses up to 54.5 GeV/c^2, for all values of the branching ratio of the charged Higgs boson into hadrons.

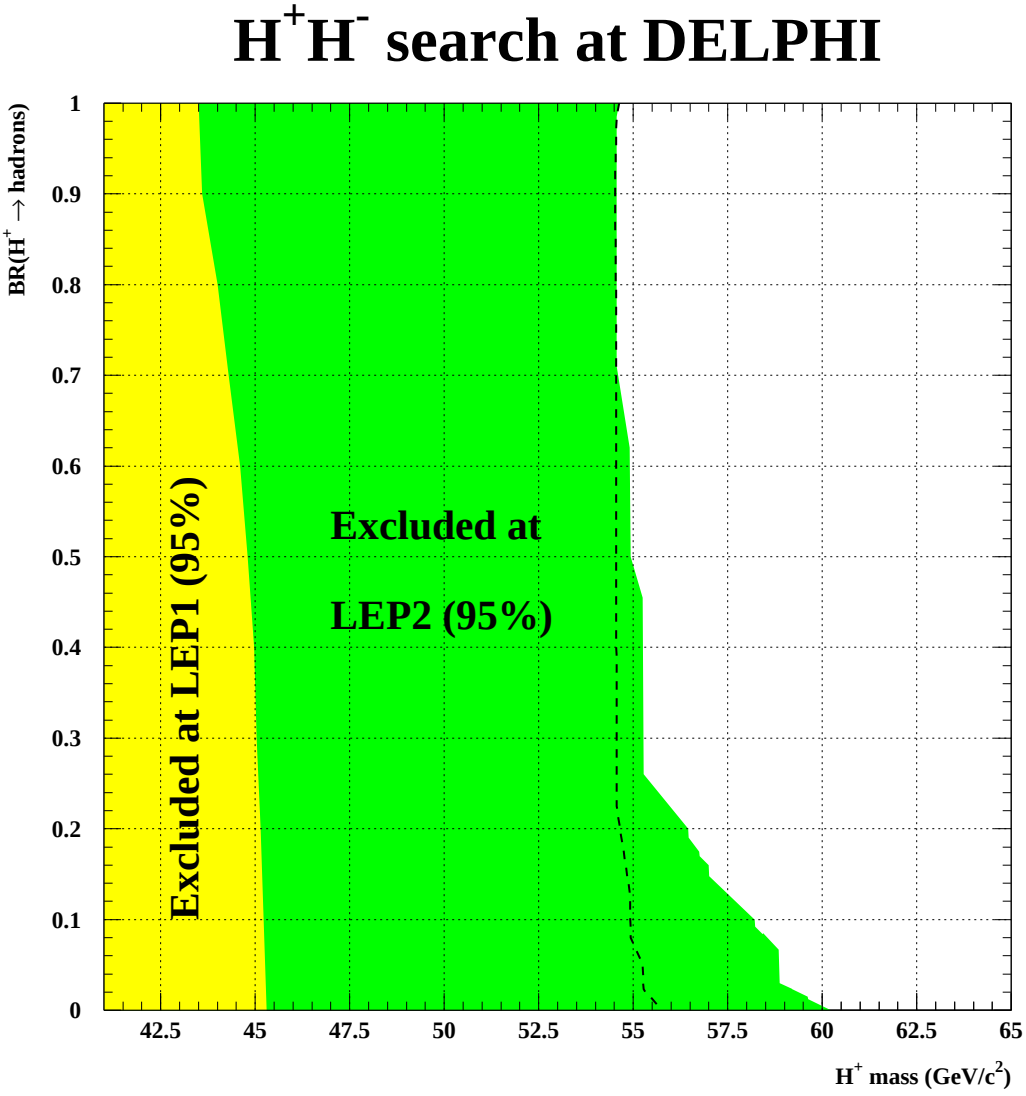

Figure 8: Exclusion limits for the existence of charged Higgs bosons as derived by this analysis. The dashed line indicates what the limit would have been if the 4 candidates expected in the leptonic channel had been seen.

The mass limit we obtain is comparable to those reported by the ALEPH [12] and OPAL [13] collaborations.

6 Acknowledgements

We are greatly indebted to our technical collaborators and to the funding authorities for their support in building and operating the DELPHI detector, and to the members of the CERN-SL division for the excellent performance of the LEP collider.

References

[1] DELPHI Coll., P. Abreu et al., 'Search for neutral and charged Higgs bosons in e^+e^- collisions at $\sqrt{s} = 161$ and 172 GeV', CERN-PPE/97-85, to appear in Z. Phys. C.
[2] DELPHI Coll., P. Aarnio et al., Nucl. Instr. and Meth. **A303** (1991) 233.
[3] DELPHI Coll., P. Abreu et al., Nucl. Instr. and Meth. **A378** (1996) 57.
[4] R.A. Fisher, 'The use of multiple measurements in taxonomic problems', Annals of Eugenics, vol. 7 (1936).
[5] M.G. Kendall and A. Stuart, 'The advanced theory of statistics', vol. 3 (1966), Griffin ed., London.
[6] C.G. Fox and S. Wolfram, Phys. Lett. **B82** (1979) 134.
[7] S. Bethke et al., Phys. Lett. **B213** (1988) 235.
[8] W.J. Murray, 'Improved B tagging using Impact Parameters', DELPHI 95-167 PHYS 581.
[9] E. Schyns, 'NEWTAG – π, K, p Tagging for Delphi RICHes', DELPHI 96-103 RICH 89.
[10] M. Battaglia and P.M. Kluit, 'Particle Identification using the RICH detectors based on the RIBMEAN package', DELPHI 96-133 RICH 90.
[11] V.F. Obraztsov, Nucl. Instr. and Meth. **A316** (1992) 388.
[12] ALEPH Coll., R. Barate et al., 'Search for charged Higgs Bosons in e^+e^- collisions at centre-of-mass energies from 130 to 172 GeV', CERN-PPE/97-129 submitted to Phys. Lett. B.
[13] OPAL Coll., 'Search for charged Higgs Bosons in e^+e^- collisions at $\sqrt{s} = 130$–172 GeV', paper 258 submitted to the 1997 EPS-HEP conference, Jerusalem.